

DESY-03-221
27th October 2018

Photoproduction of $D^{*\pm}$ mesons associated with a leading neutron

ZEUS Collaboration

Abstract

The photoproduction of $D^{*\pm}(2010)$ mesons associated with a leading neutron has been observed with the ZEUS detector in ep collisions at HERA using an integrated luminosity of 80 pb^{-1} . The neutron carries a large fraction, $x_L > 0.2$, of the incoming proton beam energy and is detected at very small production angles, $\theta_n < 0.8 \text{ mrad}$, an indication of peripheral scattering. The D^* meson is centrally produced with pseudorapidity $|\eta| < 1.5$, and has a transverse momentum $p_T > 1.9 \text{ GeV}$, which is large compared to the average transverse momentum of the neutron of 0.22 GeV . The ratio of neutron-tagged to inclusive D^* production is $8.85 \pm 0.93(\text{stat.})_{-0.61}^{+0.48}(\text{syst.}) \%$ in the photon-proton center-of-mass energy range $130 < W < 280 \text{ GeV}$. The data suggest that the presence of a hard scale enhances the fraction of events with a leading neutron in the final state.

The ZEUS Collaboration

S. Chekanov, M. Derrick, D. Krakauer, J.H. Loizides¹, S. Magill, S. Miglioranzi¹, B. Musgrave, J. Repond, R. Yoshida

Argonne National Laboratory, Argonne, Illinois 60439-4815, USA ⁿ

M.C.K. Mattingly

Andrews University, Berrien Springs, Michigan 49104-0380, USA

P. Antonioli, G. Bari, M. Basile, L. Bellagamba, D. Boscherini, A. Bruni, G. Bruni, G. Cara Romeo, L. Cifarelli, F. Cindolo, A. Contin, M. Corradi, S. De Pasquale, P. Giusti, G. Iacobucci, A. Margotti, A. Montanari, R. Nania, F. Palmonari, A. Pesci, G. Sartorelli, A. Zichichi

University and INFN Bologna, Bologna, Italy ^e

G. Aghuzumtsyan, D. Bartsch, I. Brock, S. Goers, H. Hartmann, E. Hilger, P. Irrgang, H.-P. Jakob, O. Kind, U. Meyer, E. Paul², J. Rautenberg, R. Renner, A. Stifutkin, J. Tandler, K.C. Voss, M. Wang, A. Weber³

Physikalisches Institut der Universität Bonn, Bonn, Germany ^b

D.S. Bailey⁴, N.H. Brook, J.E. Cole, G.P. Heath, T. Namsoo, S. Robins, M. Wing
H.H. Wills Physics Laboratory, University of Bristol, Bristol, United Kingdom ^m

M. Capua, A. Mastroberardino, M. Schioppa, G. Susinno

Calabria University, Physics Department and INFN, Cosenza, Italy ^e

J.Y. Kim, Y.K. Kim, J.H. Lee, I.T. Lim, M.Y. Pac⁵

Chonnam National University, Kwangju, Korea ^g

A. Caldwell⁶, M. Helbich, X. Liu, B. Mellado, Y. Ning, S. Paganis, Z. Ren, W.B. Schmidke, F. Sciulli

Nevis Laboratories, Columbia University, Irvington on Hudson, New York 10027 ^o

J. Chwastowski, A. Eskreys, J. Figiel, A. Galas, K. Olkiewicz, P. Stopa, L. Zawiejski
Institute of Nuclear Physics, Cracow, Poland ⁱ

L. Adamczyk, T. Bold, I. Grabowska-Bold⁷, D. Kisielewska, A.M. Kowal, M. Kowal, T. Kowalski, M. Przybycień, L. Suszycki, D. Szuba, J. Szuba⁸

Faculty of Physics and Nuclear Techniques, AGH-University of Science and Technology, Cracow, Poland ^p

A. Kotański⁹, W. Słomiński

Department of Physics, Jagellonian University, Cracow, Poland

V. Adler, U. Behrens, I. Bloch, K. Borras, V. Chiochia, D. Dannheim, G. Drews, J. Fourletova, U. Fricke, A. Geiser, P. Göttlicher¹⁰, O. Gutsche, T. Haas, W. Hain, S. Hillert¹¹, B. Kahle, U. Kötz, H. Kowalski¹², G. Kramberger, H. Labes, D. Lelas, H. Lim, B. Löhr, R. Mankel, I.-A. Melzer-Pellmann, C.N. Nguyen, D. Notz, A.E. Nuncio-Quiroz, A. Polini, A. Raval, L. Rurua, U. Schneekloth, U. Stösslein, G. Wolf, C. Youngman, W. Zeuner
Deutsches Elektronen-Synchrotron DESY, Hamburg, Germany

S. Schlenstedt
DESY Zeuthen, Zeuthen, Germany

G. Barbagli, E. Gallo, C. Genta, P. G. Pelfer
University and INFN, Florence, Italy^e

A. Bamberger, A. Benen, F. Karstens, D. Dobur, N.N. Vlasov
Fakultät für Physik der Universität Freiburg i.Br., Freiburg i.Br., Germany^b

M. Bell, P.J. Bussey, A.T. Doyle, J. Ferrando, J. Hamilton, S. Hanlon, D.H. Saxon, I.O. Skillicorn
Department of Physics and Astronomy, University of Glasgow, Glasgow, United Kingdom^m

I. Gialas
Department of Engineering in Management and Finance, Univ. of Aegean, Greece

T. Carli, T. Gosau, U. Holm, N. Krumnack, E. Lohrmann, M. Milite, H. Salehi, P. Schleper, S. Stonjek¹¹, K. Wichmann, K. Wick, A. Ziegler, Ar. Ziegler
Hamburg University, Institute of Exp. Physics, Hamburg, Germany^b

C. Collins-Tooth, C. Foudas, R. Gonçalo¹³, K.R. Long, A.D. Tapper
Imperial College London, High Energy Nuclear Physics Group, London, United Kingdom^m

P. Cloth, D. Filges
Forschungszentrum Jülich, Institut für Kernphysik, Jülich, Germany

M. Kataoka¹⁴, K. Nagano, K. Tokushuku¹⁵, S. Yamada, Y. Yamazaki
Institute of Particle and Nuclear Studies, KEK, Tsukuba, Japan^f

A.N. Barakbaev, E.G. Boos, N.S. Pokrovskiy, B.O. Zhautykov
Institute of Physics and Technology of Ministry of Education and Science of Kazakhstan, Almaty, Kazakhstan

D. Son
Kyungpook National University, Center for High Energy Physics, Daegu, South Korea^g

K. Piotrkowski

Institut de Physique Nucléaire, Université Catholique de Louvain, Louvain-la-Neuve, Belgium

F. Barreiro, C. Glasman¹⁶, O. González, L. Labarga, J. del Peso, E. Tassi, J. Terrón, M. Vázquez, M. Zambrana

Departamento de Física Teórica, Universidad Autónoma de Madrid, Madrid, Spain^l

M. Barbi, F. Corriveau, S. Gliga, J. Lainesse, S. Padhi, D.G. Stairs, R. Walsh

Department of Physics, McGill University, Montréal, Québec, Canada H3A 2T8^a

T. Tsurugai

Meiji Gakuin University, Faculty of General Education, Yokohama, Japan^f

A. Antonov, P. Danilov, B.A. Dolgoshein, D. Gladkov, V. Sosnovtsev, S. Suchkov

Moscow Engineering Physics Institute, Moscow, Russia^j

R.K. Dementiev, P.F. Ermolov, Yu.A. Golubkov¹⁷, I.I. Katkov, L.A. Khein, I.A. Korzhavina, V.A. Kuzmin, B.B. Levchenko¹⁸, O.Yu. Lukina, A.S. Proskuryakov, L.M. Shcheglova, S.A. Zotkin

Moscow State University, Institute of Nuclear Physics, Moscow, Russia^k

N. Coppola, S. Grijpink, E. Koffeman, P. Kooijman, E. Maddox, A. Pellegrino, S. Schagen, H. Tiecke, J.J. Velthuis, L. Wiggers, E. de Wolf

NIKHEF and University of Amsterdam, Amsterdam, Netherlands^h

N. Brümmner, B. Bylsma, L.S. Durkin, T.Y. Ling

Physics Department, Ohio State University, Columbus, Ohio 43210ⁿ

A.M. Cooper-Sarkar, A. Cottrell, R.C.E. Devenish, B. Foster, G. Grzelak, C. Gwenlan¹⁹, S. Patel, P.B. Straub, R. Walczak

Department of Physics, University of Oxford, Oxford United Kingdom^m

A. Bertolin, R. Brugnera, R. Carlin, F. Dal Corso, S. Dusini, A. Garfagnini, S. Limentani, A. Longhin, A. Parenti, M. Posocco, L. Stanco, M. Turcato

Dipartimento di Fisica dell'Università and INFN, Padova, Italy^e

E.A. Heaphy, F. Metlica, B.Y. Oh, J.J. Whitmore²⁰

Department of Physics, Pennsylvania State University, University Park, Pennsylvania 16802^o

Y. Iga

Polytechnic University, Sagamihara, Japan^f

G. D'Agostini, G. Marini, A. Nigro

Dipartimento di Fisica, Università 'La Sapienza' and INFN, Rome, Italy^e

C. Cormack²¹, J.C. Hart, N.A. McCubbin
Rutherford Appleton Laboratory, Chilton, Didcot, Oxon, United Kingdom^m

C. Heusch
*University of California, Santa Cruz, California 95064, USA*ⁿ

I.H. Park
Department of Physics, Ewha Womans University, Seoul, Korea

N. Pavel
Fachbereich Physik der Universität-Gesamthochschule Siegen, Germany

H. Abramowicz, A. Gabareen, S. Kananov, A. Kreisel, A. Levy
Raymond and Beverly Sackler Faculty of Exact Sciences, School of Physics, Tel-Aviv University, Tel-Aviv, Israel^d

M. Kuze
Department of Physics, Tokyo Institute of Technology, Tokyo, Japan^f

T. Fusayasu, S. Kagawa, T. Kohno, T. Tawara, T. Yamashita
Department of Physics, University of Tokyo, Tokyo, Japan^f

R. Hamatsu, T. Hirose², M. Inuzuka, H. Kaji, S. Kitamura²², K. Matsuzawa
Tokyo Metropolitan University, Department of Physics, Tokyo, Japan^f

M.I. Ferrero, V. Monaco, R. Sacchi, A. Solano
Università di Torino and INFN, Torino, Italy^e

M. Arneodo, M. Ruspa
Università del Piemonte Orientale, Novara, and INFN, Torino, Italy^e

T. Koop, J.F. Martin, A. Mirea
Department of Physics, University of Toronto, Toronto, Ontario, Canada M5S 1A7^a

J.M. Butterworth²³, R. Hall-Wilton, T.W. Jones, M.S. Lightwood, M.R. Sutton⁴, C. Targett-Adams
Physics and Astronomy Department, University College London, London, United Kingdom^m

J. Ciborowski²⁴, R. Ciesielski²⁵, P. Łuźniak²⁶, R.J. Nowak, J.M. Pawlak, J. Sztuk²⁷, T. Tymieniecka²⁸, A. Ukleja²⁸, J. Ukleja²⁹, A.F. Żarnecki
Warsaw University, Institute of Experimental Physics, Warsaw, Poland^q

M. Adamus, P. Plucinski
Institute for Nuclear Studies, Warsaw, Poland^q

Y. Eisenberg, L.K. Gladilin³⁰, D. Hochman, U. Karshon M. Riveline
Department of Particle Physics, Weizmann Institute, Rehovot, Israel^c

D. Kçira, S. Lammers, L. Li, D.D. Reeder, M. Rosin, A.A. Savin, W.H. Smith
Department of Physics, University of Wisconsin, Madison, Wisconsin 53706, USA ⁿ

A. Deshpande, S. Dhawan
Department of Physics, Yale University, New Haven, Connecticut 06520-8121, USA ⁿ

S. Bhadra, C.D. Catterall, S. Fourletov, G. Hartner, S. Menary, M. Soares, J. Standage
Department of Physics, York University, Ontario, Canada M3J 1P3 ^a

- ¹ also affiliated with University College London, London, UK
- ² retired
- ³ self-employed
- ⁴ PPARC Advanced fellow
- ⁵ now at Dongshin University, Naju, Korea
- ⁶ now at Max-Planck-Institut für Physik, München, Germany
- ⁷ partly supported by Polish Ministry of Scientific Research and Information Technology, grant no. 2P03B 122 25
- ⁸ partly supp. by the Israel Sci. Found. and Min. of Sci., and Polish Min. of Scient. Res. and Inform. Techn., grant no.2P03B12625
- ⁹ supported by the Polish State Committee for Scientific Research, grant no. 2 P03B 09322
- ¹⁰ now at DESY group FEB
- ¹¹ now at Univ. of Oxford, Oxford/UK
- ¹² on leave of absence at Columbia Univ., Nevis Labs., N.Y., US A
- ¹³ now at Royal Holloway University of London, London, UK
- ¹⁴ also at Nara Women's University, Nara, Japan
- ¹⁵ also at University of Tokyo, Tokyo, Japan
- ¹⁶ Ramón y Cajal Fellow
- ¹⁷ now at HERA-B
- ¹⁸ partly supported by the Russian Foundation for Basic Research, grant 02-02-81023
- ¹⁹ PPARC Postdoctoral Research Fellow
- ²⁰ on leave of absence at The National Science Foundation, Arlington, VA, USA
- ²¹ now at Univ. of London, Queen Mary College, London, UK
- ²² present address: Tokyo Metropolitan University of Health Sciences, Tokyo 116-8551, Japan
- ²³ also at University of Hamburg, Alexander von Humboldt Fellow
- ²⁴ also at Łódź University, Poland
- ²⁵ supported by the Polish State Committee for Scientific Research, grant no. 2 P03B 07222
- ²⁶ Łódź University, Poland
- ²⁷ Łódź University, Poland, supported by the KBN grant 2P03B12925
- ²⁸ supported by German Federal Ministry for Education and Research (BMBF), POL 01/043
- ²⁹ supported by the KBN grant 2P03B12725
- ³⁰ on leave from MSU, partly supported by University of Wisconsin via the U.S.-Israel BSF

- ^a supported by the Natural Sciences and Engineering Research Council of Canada (NSERC)
- ^b supported by the German Federal Ministry for Education and Research (BMBF), under contract numbers HZ1GUA 2, HZ1GUB 0, HZ1PDA 5, HZ1VFA 5
- ^c supported by the MINERVA Gesellschaft für Forschung GmbH, the Israel Science Foundation, the U.S.-Israel Binational Science Foundation and the Benozio Center for High Energy Physics
- ^d supported by the German-Israeli Foundation and the Israel Science Foundation
- ^e supported by the Italian National Institute for Nuclear Physics (INFN)
- ^f supported by the Japanese Ministry of Education, Culture, Sports, Science and Technology (MEXT) and its grants for Scientific Research
- ^g supported by the Korean Ministry of Education and Korea Science and Engineering Foundation
- ^h supported by the Netherlands Foundation for Research on Matter (FOM)
- ⁱ supported by the Polish State Committee for Scientific Research, grant no. 620/E-77/SPB/DESY/P-03/DZ 117/2003-2005
- ^j partially supported by the German Federal Ministry for Education and Research (BMBF)
- ^k partly supported by the Russian Ministry of Industry, Science and Technology through its grant for Scientific Research on High Energy Physics
- ^l supported by the Spanish Ministry of Education and Science through funds provided by CICYT
- ^m supported by the Particle Physics and Astronomy Research Council, UK
- ⁿ supported by the US Department of Energy
- ^o supported by the US National Science Foundation
- ^p supported by the Polish State Committee for Scientific Research, grant no. 112/E-356/SPUB/DESY/P-03/DZ 116/2003-2005, 2 P03B 13922
- ^q supported by the Polish State Committee for Scientific Research, grant no. 115/E-343/SPUB-M/DESY/P-03/DZ 121/2001-2002, 2 P03B 07022

1 Introduction

Events containing a leading neutron have been studied in ep collisions at HERA [1–4]. The neutrons carry a large fraction of the incoming proton beam energy, $x_L > 0.2$, and are produced at very small scattering angles, $\theta_n < 0.8$ mrad, indicative of a peripheral process.

The small transverse momenta (p_T) which characterize leading baryon production processes imply a soft scale, which means that a non-perturbative approach is required to model such events. Particle-exchange models within Regge theory [5], in particular the one-pion-exchange model (OPE) [6–8], are often applied to describe leading neutron production. Charm production, in contrast, can be used to investigate parton dynamics because the charm-quark mass provides the hard scale necessary to ensure the applicability of perturbative Quantum Chromodynamics (pQCD). Therefore the study of charm production in events with a leading neutron gives information on the interplay between soft and hard scales.

This letter presents measurements of $D^{*\pm}$ photoproduction associated with a leading neutron. Differential cross sections and ratios to inclusive $D^{*\pm}$ photoproduction are reported. These results extend previous ZEUS studies [1,3,4] of leading-neutron production in dijet and inclusive photoproduction and deep inelastic scattering.

2 Charm and neutron production

An important process in charm photoproduction is Boson-Gluon Fusion (BGF). At leading order this corresponds to the direct component where the photon couples directly to a high-transverse-momentum $c\bar{c}$ pair which interacts with a gluon from the proton. Another contribution to the cross section comes from the resolved component, where the photon acts as a source of partons, interacting with the proton mostly via charm excitation processes, $cq \rightarrow cq$ and $cg \rightarrow cg$ [9].

The mechanism for leading neutron production is not well understood. In the following subsections some models for neutron production are briefly discussed.

2.1 Fragmentation models

In fragmentation models of partons into hadrons, such as the cluster model [10] or the Lund string model [11], a certain fraction of neutrons is expected in the final state. In this case the leading neutrons are produced by fragmentation of the proton remnant using

the same mechanism as is used for the other final state hadrons. Such models predict a softer x_L distribution than that measured [1–4].

2.2 One-pion-exchange model

Previous studies have shown that particle-exchange models [6–8, 12–15] describe data on leading neutron production both at HERA [1–4] and at hadroproduction experiments [16–25]. In such models the transition amplitude for $p \rightarrow n$ is dominated by OPE and the electroproduction cross section can be written as the convolution of a function describing the splitting of a proton into a πn system, i.e. the pion flux factor $f_{\pi/p}(x_L, t)$, and the $e\pi$ cross section:

$$\frac{d\sigma_{ep \rightarrow e'nX}}{dx_L dt} = f_{\pi/p}(x_L, t) \sigma^{e\pi}(s'), \quad (1)$$

where t is the squared four-momentum transfer at the proton vertex, $s' = s(1 - x_L)$ is the squared center-of-mass energy of the $e\pi$ system and s is that of the ep .

The flux factors found in the literature can be expressed in general as [8, 15]

$$f_{\pi/p}(x_L, t) = \frac{1}{4\pi} \frac{2g_{p\pi p}^2}{4\pi} \frac{-t}{(t - m_\pi^2)^2} (1 - x_L)^{1-2\alpha(t)} [F(x_L, t)]^2, \quad (2)$$

where $g_{p\pi p}^2/(4\pi) \sim 14.5$ is the $p\pi p$ coupling constant, m_π is the pion mass and $\alpha(t)$ is defined below. The form-factor $F(x_L, t)$ accounts for the finite size of the nucleon and pion. Examples of flux factor parametrizations are:

- f_1 [26]:

$$F(x_L, t) = \exp \left[R^2 \frac{(t - m_\pi^2)}{(1 - x_L)} \right], \quad \alpha(t) = 0, \quad (3)$$

where $R = 0.6 \text{ GeV}^{-1}$ and $F(x_L, t)$ is the light-cone form factor.

- f_2 [8]:

$$F(x_L, t) = 1, \quad \alpha(t) = \alpha_\pi(t) \quad (4)$$

where $\alpha_\pi(t) \simeq t$ (with t in GeV^2) is the Regge trajectory of the pion.

- f_3 [27]:

$$F(x_L, t) = \exp[b(t - m_\pi^2)], \quad \alpha(t) = \alpha_\pi(t) \quad (5)$$

where $b = 0.3 \text{ GeV}^{-2}$ and $F(x_L, t)$ is the exponential form factor ;

- f_4 [28]:

$$F(x_L, t) = \frac{(1 - m_\pi^2/\Lambda^2)}{(1 - t^2/\Lambda^2)}, \quad \alpha(t) = 0 \quad (6)$$

where $\Lambda = 0.25 \text{ GeV}$ and $F(x_L, t)$ is the monopole form factor.

The term $\sigma^{e\pi}$ in Eq. (1) involve the parton distribution in the pion. Charm production in association with a leading neutron is potentially sensitive to the gluon content of the pion in OPE models via the BGF process. Parametrizations for the pionic parton distribution function (PDF) available in the literature were obtained by performing fits to πN scattering data, assuming some parametrization for the nucleon structure function. Examples of such parametrizations are those by Owens [29] which come from fits on J/Ψ and dimuon production data. The more recent GRV parametrizations [30] assume a valence-like structure for the pion at a certain low scale. This distribution is dynamically evolved and the results combined with the constraints imposed by prompt photon production data on the pionic gluon density.

2.3 Rescattering effects

From the factorization hypothesis expressed in Eq. (1), it is expected that the ratios, r , of neutron-tagged to inclusive cross sections for different electroproduction processes are about the same. Most of the dependence of the cross sections on the kinematics of the processes cancels; remaining differences can be attributed to differences between the pion and proton energies and their PDFs. However, larger differences than these may arise from neutron absorption, which can occur through rescattering of the neutron on the exchanged photon [14, 31]. With increasing size of the virtual photon more rescattering may be expected.

Inclusive photoproduction cross sections are well described by vector meson dominance models [32–34], where the dipole associated with the photon is of hadronic size. In dijet photoproduction, the presence of the hard scale given by the transverse energy of the jets implies smaller dipole size. In the infinite-momentum frame the smaller dipole size corresponds to the enhancement of the direct photon component at high transverse energy E_T . Such an enhancement has been observed at HERA [35]. Absorptive effects in dijet photoproduction, therefore, are expected to be smaller than those in inclusive photoproduction. In the case of charm photoproduction, an additional hard scale is provided by the mass of the charm quark. Previous ZEUS measurements have shown that requiring the presence of charm further suppresses the resolved component [36] compared to inclusive dijet photoproduction. Therefore rescattering in D^* photoproduction may be further suppressed in comparison to dijet photoproduction. In deep inelastic scattering (DIS), at sufficiently high photon virtuality, little rescattering should occur. Within such a picture, therefore, the ratios are expected to have the following relationship:

$$r^{\gamma p} < r^{\text{jj}} < r^{D^*} \lesssim r^{\text{DIS}}.$$

3 Experimental conditions

The integrated luminosity of $80.2 \pm 1.8 \text{ pb}^{-1}$ used for this measurement was collected at the ep collider HERA with the ZEUS detector during 1998 - 2000, when HERA collided 27.5 GeV electrons or positrons¹ with 920 GeV protons, giving a center-of-mass energy of 318 GeV.

A detailed description of the ZEUS detector can be found elsewhere [37]. A brief outline of the components that are most relevant for this analysis is given below. Charged particles are tracked in the central tracking detector (CTD) [38], which operates in a magnetic field of 1.43 T provided by a thin superconducting solenoid. The central tracking detector consists of 72 cylindrical drift chamber layers, organized in nine superlayers covering the polar-angle² region $15^\circ < \theta < 164^\circ$. The transverse-momentum resolution for full-length tracks is $\sigma(p_T)/p_T = 0.0058p_T \oplus 0.0065 \oplus 0.0014/p_T$, with p_T in GeV.

The high-resolution uranium–scintillator calorimeter (CAL) [39] consists of three parts: the forward, the barrel and the rear calorimeters. Each part is subdivided transversely into towers and longitudinally into one electromagnetic section and either one (in rear) or two (in barrel and forward) hadronic sections. The smallest subdivision of the calorimeter is called a cell. The calorimeter energy resolutions, as measured under test-beam conditions, are $\sigma(E)/E = 0.18/\sqrt{E}$ for electrons and $\sigma(E)/E = 0.35/\sqrt{E}$ for hadrons, with E in GeV.

The forward neutron calorimeter (FNC) [40,41] was installed in the HERA tunnel at $\theta = 0$ degrees and at $Z = 106$ m from the interaction point in the proton-beam direction. It is a lead-scintillator calorimeter which is segmented longitudinally into a front section, seven interaction lengths deep, and a rear section, three interaction lengths deep. The front section is divided vertically into 14 towers, allowing the separation of electromagnetic and hadronic showers from the energy-weighted vertical width of the showers. The energy resolution for neutrons, as measured in a beam test, is $\sigma(E_n)/E_n = 0.65/\sqrt{E_n}$, with neutron energy, E_n , in GeV. Three planes of veto counters are used to reject events in which particles had interacted with the inactive material in front of the FNC. Magnet apertures limit the FNC acceptance to neutrons with production angles less than 0.8 mrad, which corresponds to transverse momenta $p_T \leq E_n \theta_{\max} = 0.74x_L$ GeV. The mean value of p_T for the data is 0.22 GeV.

The luminosity was determined from the rate of the bremsstrahlung process $ep \rightarrow e\gamma p$,

¹ Hereafter, both e^+ and e^- are referred to as electrons.

² The ZEUS coordinate system is a right-handed Cartesian system, with the Z axis pointing in the proton beam direction, referred to as the “forward direction”, and the X axis pointing left towards the center of HERA. The coordinate origin is at the nominal interaction point.

where the photon was measured with a lead-scintillator calorimeter [42, 43] located at $Z = -107$ m.

4 Kinematics

The kinematics of photoproduction at HERA are specified by the photon virtuality, Q^2 , and the photon-proton center-of-mass energy, W . The electron-proton center-of-mass energy, \sqrt{s} , is related to W by $W^2 = ys$ where y is the fraction of the electron beam energy carried by the photon in the proton rest frame.

To describe the process $ep \rightarrow e'D^{*\pm}nX$, four additional variables are used: two for the neutron and two for the charmed meson. They are:

- (x_L, θ_n) , the fractional energy and production angle of the produced neutron; only about half of the data have a θ_n measurement, therefore all results discussed here are integrated over this variable up to the maximum accepted angle of 0.8 mrad;
- (p_T, η) , the transverse momentum and pseudorapidity of the produced $D^{*\pm}$ meson.

The measurement was performed in the following kinematic region: $Q^2 < 1$ GeV², $130 < W < 280$ GeV, $|\eta(D^*)| < 1.5$, $p_T(D^*) > 1.9$ GeV, $x_L > 0.2$ and $\theta_n < 0.8$ mrad.

5 Event Selection

5.1 Trigger

A three-level trigger system was used to select events online [37, 44]. The selection was based on energy deposits, tracking and event timing. The FNC was not used in the trigger.

5.2 Photoproduction selection

Photoproduction events were selected offline using cuts based on the reconstructed primary vertex position, CAL energy deposits and the reconstructed tracks of charged particles. Events with a well-identified electron candidate in the CAL were removed. It was required that $\sum_i (E_i - p_{Z,i}) > 7$ GeV, where the sum runs over all CAL cells and $p_{Z,i}$ is the Z component of the momentum vector assigned to each cell of energy E_i . Tracking and CAL information was combined to form energy flow objects (EFOs) [45, 46]. A cut was made on the Jacquet-Blondel [47] estimator of W^2 , $W_{\text{JB}}^2 = y_{\text{JB}}s$, where $y_{\text{JB}} = \sum_i (E_i - E_{Z,i})/2E_e$,

and $E_{Z,i} = E_i \cos \theta_i$; E_i is the energy of EFO i with polar angle θ_i with respect to the measured Z -vertex of the event. The sum runs over all EFOs. It was required that $W_{\text{JB}} < 265$ GeV. These cuts correspond to a true W range of $130 < W < 280$ GeV and $Q^2 < 1$ GeV² with the median $Q^2 \approx 10^{-3}$ GeV².

5.3 $D^{*\pm}(2010)$ reconstruction

The inclusive charm sample was selected by identifying events containing a charmed meson. The $D^{*\pm}$ selection cuts are based on the decay channel: $D^{*+} \rightarrow (D^0 \rightarrow K^-\pi^+)\pi_s^+$ (+ charge conjugate), where π_s indicates the “slow” pion [48]. Only tracks assigned to the primary event vertex and with hits in at least three superlayers of the CTD were considered. The combinatorial background was reduced and the kinematic phase space defined by requiring: the transverse momentum of the kaon and pion candidates to satisfy $p_T(K) > 0.45$ GeV, $p_T(\pi) > 0.45$ GeV and $p_T(\pi_s) > 0.12$ GeV; the transverse momentum of the $D^{*\pm}$ to be greater than 1.9 GeV and the pseudorapidity of the $D^{*\pm}$ to satisfy $|\eta(D^{*\pm})| < 1.5$.

Since no particle identification was performed, the K and π masses were alternately attributed to the decay products of the candidate D^0 meson. Those D^0 candidates that had an invariant mass between 1.80 and 1.92 GeV were required to have a mass difference $\Delta M = M(K\pi\pi_s) - M(K\pi)$ between 0.1435 and 0.1475 GeV. The combinatorial background was estimated from the mass-difference distribution for wrong-charge combinations, in which both tracks forming the D^0 candidates have the same charge and the third track has the opposite charge.

5.4 Neutron reconstruction

Events with a leading neutron were selected from the inclusive charm sample by requiring a large energy deposit ($E_n > 184$ GeV) in the FNC. Protons, photons, and neutrons are separated by their position in the detector, as well as by the shower width. Scattered protons are deflected by the HERA magnets and strike the top part of the FNC. Photons can be identified and removed from the sample because the transverse spread of electromagnetic showers is much less than that of hadronic showers.

Events with particles that started to shower before reaching the FNC were removed by requiring that the scintillator veto counter had an energy deposit below that of a minimum-ionizing particle. Events with wide showers, inconsistent with originating from a single high-energy hadron, were removed.

5.5 Final event sample

The ΔM distribution for the neutron-tagged sample is shown in Fig. 1, along with the wrong-charge combinations. A prominent $D^{*\pm}$ signal is observed. The signal observed in the $M(K\pi)$ distribution for events within the mass window $0.1435 < \Delta M < 0.1475$ GeV is shown as an inset.

After the wrong-charge background subtraction, 298 ± 31 $D^{*\pm}$ mesons were found. The same background subtraction procedure, applied to the inclusive $D^{*\pm}$ sample, gave $14\,743 \pm 253$ events.

6 Monte Carlo simulation and acceptance corrections

A GEANT-based [49] Monte Carlo (MC) simulation was used to calculate selection efficiencies and correction factors for the charmed meson. Three different event generators were used: RAPGAP 2.08/06 [50] for evaluating the nominal corrections, HERWIG 6.301 [51] and PYTHIA 6.156 [52] as systematic checks. RAPGAP and PYTHIA use the Lund string model for hadronization. HERWIG uses a cluster model. The events generated with RAPGAP for acceptance calculations were produced using OPE for the production of the leading neutron, with the pion flux factor from Eqs. (2) and (3) and the GRV parametrization [30] for the pion PDF. Inclusive RAPGAP, employing the Lund string model instead of OPE for neutron production, was produced for comparisons to the final measurements. The leading neutron is also produced via the Lund string model in PYTHIA. In HERWIG, it is produced via the cluster model. The proton PDFs parametrizations used were CTEQ5L [53] for PYTHIA and HERWIG, and CTEQ4D [54] for inclusive RAPGAP. The photon PDF GRV-G LO [55] was used in PYTHIA and HERWIG, and GRS LO [56] in RAPGAP. The mass of the charm quark was set to 1.5 GeV. The fraction of c quarks hadronizing to a D^* meson was set to $f(c \rightarrow D^*) = 0.235$ [57]. Both direct and resolved photon processes for charm production were generated, in proportion to their predicted cross sections. Effects of neutron rescattering were not taken into account in the simulation.

For all the MC samples used to evaluate the acceptances, events with at least one $D^{*\pm}$ decaying in the appropriate decay channel were selected and passed through the ZEUS detector and trigger simulations as well as the event-reconstruction package.

Since the D^* and neutron were independently detected and their kinematics largely uncorrelated, the acceptances for the two particles factorize. The selection efficiencies and correction factors for the neutron calculated for previous analyses [4] were used. The overall acceptance of the FNC, which includes the beam-line geometry and the angular distribution of the neutrons, is about 25% for neutrons with $x_L > 0.2$ and $\theta_n < 0.8$ mrad.

The differential cross section for $D^{*\pm}$ photoproduction associated with a leading neutron was evaluated in terms of a given variable Y as $d\sigma/dY = N/(A_{\text{FNC}} \cdot A_{D^*} \cdot B \cdot \Delta Y)$ where N is the number of D^* found in the final sample in a bin of size ΔY , A_{FNC} is the acceptance for the neutron detection in the FNC, A_{D^*} is the acceptance for the D^* reconstruction and B is the branching ratio for the selected decay mode. A value of $B = 2.57\%$ [58] was used.

7 Systematic uncertainties

For the $D^{*\pm}$ measurement the major sources of systematic uncertainty are listed below (the relative uncertainty on $D^{*\pm}$ acceptance is shown in parentheses):

- the selection of photoproduction events and $D^{*\pm}$ candidates. Variations were made in the W_{JB} (+4.5 %) and Z -vertex ($^{+1.5}_{-0.3}$ %) cuts;
- the p_T of the pion and kaon cuts. These were varied according to their resolutions ($^{+1.2}_{-1.7}$ %);
- variation of the mass windows. The ΔM window used for the extraction of the $D^{*\pm}$ was widened symmetrically by 0.5 MeV. The $M(D^0)$ window was widened and reduced symmetrically by 5 MeV ($^{+3.4}_{-3.6}$ %);
- the ΔM region for the normalization of the wrong-charged combinations. This was changed from 0.15 – 0.165 GeV to 0.15 – 0.163 GeV (+2.4 %);
- the MC model dependence. HERWIG (−4.8 %) and PYTHIA (+2 %) were used instead of RAPGAP;
- the fraction of resolved photon events in the MC was lowered by 20% and raised by 10 % ($^{+0.8}_{-1.8}$ %);
- the CAL energy scale. This was varied within its uncertainty of $\pm 3\%$ (± 0.9 %).

An extensive discussion of the systematic effects related to the neutron measurement is given elsewhere [4]. Here, the major sources of systematic uncertainty and their effect on the FNC acceptance (shown in parentheses) is listed:

- the uncertainty in the angular distribution of the neutrons ($\pm 4\%$ for $x_L < 0.82$, $\pm 7\%$ for $x_L > 0.82$);
- the uncertainty in the overall FNC energy scale of $\pm 2\%$ (less than 4% effect for $x_L < 0.82$, $^{+14}_{-16}\%$ for $x_L > 0.82$);
- the normalization uncertainty arising from proton-beam-gas interactions overlapping with photoproduction events, the uncertainty in the amount of dead material in the beam line, and the uncertainties from the veto cuts ($\pm 5\%$).

All above errors were added in quadrature separately for the positive and negative variations to determine the overall systematic uncertainty. The overall normalization has additional uncertainties of 2.2% due to the luminosity measurement and 2.5% due to the knowledge of branching ratios.

Sources of systematic uncertainty in the ratio measurement were studied in a similar manner to those for the cross-section measurements. There is a cancellation between the common systematic uncertainties originating from the selection of inclusive photoproduction events, the selection of $D^{*\pm}$ candidates and the background estimation. The remaining contributions are those from the model dependence of the acceptance corrections used in the evaluation of the inclusive $D^{*\pm}$ photoproduction cross sections and from the neutron measurement uncertainties.

8 Results

The integrated cross section for the reaction $ep \rightarrow e'D^{*\pm}nX$ in the kinematic region $Q^2 < 1 \text{ GeV}^2$, $130 < W < 280 \text{ GeV}$, $|\eta(D^*)| < 1.5$, $p_T(D^*) > 1.9 \text{ GeV}$, $x_L > 0.2$ and $\theta_n < 0.8 \text{ mrad}$ is

$$2.08 \pm 0.22(\text{stat.})_{-0.18}^{+0.12}(\text{syst.}) \pm 0.05(\text{B.R.}) \text{ nb},$$

where the final uncertainty arises from the uncertainty of the branching ratios for the D^* and D^0 . The luminosity uncertainty was included in the systematic uncertainty. The predicted cross sections from the models are 3.0 nb for HERWIG, 4.6 nb for PYTHIA, 2.6 nb for inclusive RAPGAP and 2.0 nb for RAPGAP with OPE.

Table 1 and Fig. 2 show the differential cross sections for neutron-tagged $D^{*\pm}$ production as a function of W , $p_T(D^*)$ and $\eta(D^*)$. The differential cross section as a function of x_L is shown in Table 1 and Fig. 3.

The inclusive $D^{*\pm}$ cross section was measured and found to agree with previous measurements [36] in a similar kinematic range. Table 2 and Fig. 4 show the measured ratios of neutron-tagged to inclusive $D^{*\pm}$ production as a function of different kinematic variables. Over the whole measured kinematic range the ratio is

$$r^{D^*} = 8.85 \pm 0.93(\text{stat.})_{-0.61}^{+0.48}(\text{syst.}) \%$$

which is shown superposed on Fig. 4. The χ^2 per degree of freedom with respect to the overall ratio are 0.27, 1.65 and 0.09 for the W , $p_T(D^*)$ and $\eta(D^*)$ distributions. Within the experimental uncertainties neutron-tagged $D^{*\pm}$ production is compatible with being a constant fraction of inclusive $D^{*\pm}$ production, independent of the $D^{*\pm}$ kinematics.

9 Discussion

The experimental results in Figs. 2 and 3a are compared to the predictions, normalized to the data, of the MC models RAPGAP with OPE for leading-neutron production, HERWIG, PYTHIA and inclusive RAPGAP. In Fig. 2, the agreement in shape between data and MC models is satisfactory in all cases. Fig. 3a, however, shows that only RAPGAP with OPE agrees with the measured neutron energy distribution seen in the data. A similar result was obtained in the study of neutron-tagged dijet photoproduction [3].

In principle the data allow the pion PDF to be probed in the range of the parton fractional momenta $10^{-3} < x_\pi < 10^{-2}$. Figure 3b shows the differential cross section in x_L compared to the predicted cross sections from RAPGAP with OPE, based on different parametrizations for the pion structure function: GRV set 1 and Owens sets 1 and 2. The data have little sensitivity, as in the case of neutron-tagged dijet photoproduction [3], to the choice of the pion structure function. Even with an extreme choice of a pion structure function, e.g. a completely flat gluon distribution, or a parametrization identical to the proton structure function, little variation is seen in the predictions.

Figure 3c shows the data compared to the predictions of RAPGAP with OPE for the four flux factors discussed in Section 2.2. All RAPGAP distributions are normalized to the data and the resulting normalization factors are given in the figure. Fluxes f_1 and f_3 give similar results, being compatible with the data both in shape and normalization. The fluxes f_2 and f_4 are disfavored by the shape of the data, and the latter predicts cross sections almost three times smaller than data.

The independence of r^{D^*} on W , $p_T(D^*)$ and $\eta(D^*)$, shown in Fig. 4, supports the hypothesis of vertex factorization, in agreement with previous studies of leading-neutron production [1, 3, 4]. The predicted ratios from the models are: 0.24 for HERWIG, 0.29 for PYTHIA, and 0.18 for RAPGAP.

The ratio for charm production, r^{D^*} , is in agreement with the analogous ratio previously measured for neutron-tagged DIS, $Q^2 > 4 \text{ GeV}^2$ [4],

$$r^{\text{DIS}} = 8.0 \pm 0.5 \text{ \%},$$

but lies above the ratio previously measured for neutron-tagged inclusive photoproduction at $W = 207 \text{ GeV}$ [4],

$$r^{\gamma p} = 5.7 \pm 0.4 \text{ \%},$$

as expected from the rescattering effects within the OPE model (see Section 2.3). The errors quoted are the quadratic sum of the statistical and systematic uncertainties.

For photoproduced dijets the neutron-tagged to inclusive ratio has only been measured for $x_L > 0.49$. In this kinematic region, the measured $D^{*\pm}$ ratio and their corresponding

ratios previously measured for DIS, inclusive photoproduction [4], and photoproduction of dijets with transverse energy $E_T^{\text{jett}} > 6$ GeV [3] are:

$$\begin{aligned}
r^{D^*}(x_L > 0.49) &= 6.55 \pm 0.76(\text{stat.})_{-0.45}^{+0.35}(\text{syst.}) \% \\
r^{\text{DIS}}(x_L > 0.49) &= 5.8 \pm 0.3 \% \\
r^{\text{jj}}(x_L > 0.49) &= 4.9 \pm 0.4 \% \\
r^{\gamma p}(x_L > 0.49) &= 4.3 \pm 0.3 \%.
\end{aligned}$$

The results are compatible with the rescattering hypothesis described in Section 2.3.

10 Summary

The photoproduction of $D^{*\pm}$ mesons associated with a leading neutron has been studied in ep interactions at HERA in the kinematic region $Q^2 < 1$ GeV², $130 < W < 280$ GeV, $|\eta(D^*)| < 1.5$, $p_T(D^*) > 1.9$ GeV, $\theta_n < 0.8$ mrad and $x_L > 0.2$. The Monte Carlo models RAPGAP, HERWIG and PYTHIA give a satisfactory description of the $D^{*\pm}$ kinematics, but only RAPGAP with one-pion exchange satisfactorily describes the leading-neutron energy distribution. The results show sensitivity to the choice of pion flux factor. The ratio of neutron-tagged $D^{*\pm}$ photoproduction to inclusive $D^{*\pm}$ photoproduction is $r^{D^*} = 8.85 \pm 0.93(\text{stat.})_{-0.61}^{+0.48}(\text{syst.})\%$.

The ratio of neutron-tagged $D^{*\pm}$ photoproduction to inclusive $D^{*\pm}$ photoproduction is constant as a function of W , $p_T(D^*)$ and $\eta(D^*)$, in agreement with the hypothesis of vertex factorization. This ratio is consistent with the analogous ratio in deep inelastic scattering, but both are about 30% higher than the corresponding ratio for inclusive photoproduction, suggesting that the presence of a hard scale enhances the fraction of events with a leading neutron in the final state.

Acknowledgements

We thank the DESY Directorate for their strong support and encouragement, and the HERA machine group for their diligent efforts. We are grateful for the support of the DESY computing and network services. The design, construction and installation of the ZEUS detector have been made possible owing to the ingenuity and effort of many people who are not listed as authors.

References

- [1] ZEUS Coll., M. Derrick et al., Phys. Lett. **B 384**, 388 (1996).
- [2] H1 Coll., C. Adloff et al., Eur. Phys. J. **C 6**, 587 (1999).
- [3] ZEUS Coll., J. Breitweg et al., Nucl. Phys. **B 596**, 3 (2000).
- [4] ZEUS Coll., J. Breitweg et al., Nucl. Phys. **B 637**, 3 (2002).
- [5] P.D.B. Collins, *An Introduction to Regge Theory and High Energy Physics*, Cambridge University Press (1977).
- [6] H. Yukawa, Proc. Phys. Math. Soc. Japan **17**, 48 (1935).
- [7] J.D. Sullivan, Phys. Rev. **D 5**, 1732 (1972).
- [8] M. Bishari, Phys. Rev. Lett. **B 38**, 510 (1972).
- [9] ZEUS Coll., S. Chekanov et al., Phys. Lett. **B 565**, 87 (2003).
- [10] B.R. Webber, Nucl. Phys. **B 238**, 492 (1984).
- [11] B. Andersson, G. Gustafson and B. Söderberg, Z. Phys. **C 20**,317 (1983).
- [12] V.R. Zoller, Z. Phys. **C 53**, 443 (1992).
- [13] S.N. Ganguli and D.P. Roy, Phys. Rep. **67**, 201 (1980).
- [14] B.G. Zakharov and V.N. Sergeev, Sov. J. Nucl. Phys. **38**, 947 (1983);
B.G. Zakharov and V.N. Sergeev, Sov. J. Nucl. Phys. **39**, 448 (1984).
- [15] R.D. Field and G.C. Fox, Nucl. Phys. **B 80**, 367 (1974).
- [16] A.R. Erwin et al., Phys. Rev. Lett. **6**, 628 (1961).
- [17] E. Pickup, D.K. Robinson and E.O. Salant, Phys. Rev. Lett. **7**, 192 (1961);
Erratum - ibid, 472.
- [18] B. Robinson et al., Phys. Rev. Lett. **34**, 1475 (1975).
- [19] J. Engler et al., Nucl. Phys. **B 84**, 70 (1975).
- [20] W. Flauger and F. Mönnig, Nucl. Phys. **B 109**, 347 (1976).
- [21] J. Hanlon et al., Phys. Rev. Lett. **37**, 967 (1976);
J. Hanlon et al., Phys. Rev. **D 20**, 2135 (1979).
- [22] G. Hartner, Ph.D. Thesis, McGill University (1977) (unpublished).
- [23] Y. Eisenberg et al., Nucl. Phys. **B 135**, 189 (1978).
- [24] V. Blobel et al., Nucl. Phys. **B 135**, 379 (1978).
- [25] H. Abramowicz et al., Nucl. Phys. **B 166**, 62 (1980).

- [26] H. Holtmann et al., Phys. Rev. Lett. **B 338**, 363 (1994).
- [27] B. Kopeliovich, B. Povh and I. Potashnikova, Z. Phys. **C 73**, 125 (1996).
- [28] L.L. Frankfurt, L. Mankiewicz and M.I. Strikman, Z. Phys. **A 334**, 343 (1989).
- [29] J.F. Owens, Phys. Rev. **D 30**, 943 (1984).
- [30] M. Gluck, E. Reya and A. Vogt, Z. Phys. **C 53**, 651 (1992).
- [31] K.J.M. Moriarty et al., Phys. Rev. **D 16**, 130 (1976);
A.G. Azcarate, Phys. Rev. **D 17**, 3022 (1978);
N.N. Nikolaev, J. Speth and B.G. Zakharov, hep-ph/9708290 (1997);
U. D'Alesio and H.J. Pirner, Eur. Phys. J. **A 7**, 109 (2000).
- [32] T.H. Bauer et al., Rev. Mod. Phys. **50**, 261 (1978), Erratum-ibid. **51**, 407 (1979).
- [33] ZEUS Coll., S. Chekanov et al., Nucl. Phys. **B 627**, 3 (2002).
- [34] H1 Coll., S. Aid et al., Z. Phys. **C 69**, 27 (1995).
- [35] ZEUS Coll., J. Breitweg et al., Eur. Phys. J. **C 1**, 109 (1998);
ZEUS Coll., J. Breitweg et al., Eur. Phys. J. **C 11**, 35 (1999);
ZEUS Coll., S. Chekanov et al., Eur. Phys. J. **C 23**, 615 (2002);
H1 Coll., C. Adloff et al., Eur. Phys. J. **C 25**, 13 (2002).
- [36] ZEUS Coll., J. Breitweg et al., Eur. Phys. J. **C 6**, 67 (1999).
- [37] ZEUS Coll., U. Holm (ed.), *The ZEUS Detector*. Status Report (unpublished),
DESY (1993), available on <http://www-zeus.desy.de/bluebook/bluebook.html>.
- [38] N. Harnew et al., Nucl. Inst. Meth. **A 279**, 290 (1989);
B. Foster et al., Nucl. Phys. Proc. Suppl. **B 32**, 181 (1993);
B. Foster et al., Nucl. Inst. Meth. **A 338**, 254 (1994).
- [39] M. Derrick et al., Nucl. Inst. Meth. **A 309**, 77 (1991);
A. Andresen et al., Nucl. Inst. Meth. **A 309**, 101 (1991);
A. Caldwell et al., Nucl. Inst. Meth. **A 321**, 356 (1992);
A. Bernstein et al., Nucl. Inst. Meth. **A 336**, 23 (1993).
- [40] S. Bhadra et al., Nucl. Inst. Meth. **A 354**, 479 (1995).
- [41] S. Bhadra et al., Nucl. Inst. Meth. **A 394**, 121 (1997).
- [42] J. Andruszków et al., Preprint DESY-92-066, DESY (1992);
ZEUS Coll., M. Derrick et al., Z. Phys. **C 63**, 391 (1994).
- [43] J. Andruszków et al., Acta Phys. Pol. **B 32**, 2025 (2001).
- [44] W.H. Smith, K. Tokushuku and L.W. Wiggers, *Proc. Computing in High-Energy Physics (CHEP), Annecy, France, Sept. 1992*, C. Verkerk and W. Wojcik (eds.),
p. 222. CERN, Geneva, Switzerland (1992). Also in preprint DESY 92-150B.

- [45] G.M. Briskin, Ph.D. Thesis, Tel Aviv University (1998) (unpublished).
- [46] ZEUS Coll., J. Breitweg et al., *Eur. Phys. J. C* **1**, 81 (1998).
- [47] F. Jacquet and A. Blondel, *Proceedings of the Study for an ep Facility for Europe*, U. Amaldi (ed.), p. 391. Hamburg, Germany (1979). Also in preprint DESY 79/48.
- [48] S. Nussinov, *Phys. Rev. Lett.* **35**, 1672 (1975).
- [49] R. Brun et al., GEANT3, Technical Report CERN-DD/EE/84-1, CERN (1987).
- [50] H. Jung, *Comp. Phys. Comm.* **86**, 147 (1995).
- [51] G. Marchesini et al., *Comp. Phys. Comm.* **67**, 465 (1992).
- [52] T. Sjöstrand, *Comp. Phys. Comm.* **135**, 238 (2001).
- [53] CTEQ Coll., H.L. Lai et al., *Eur. Phys. J. C* **12**, 375 (2000).
- [54] H.L. Lai et al., *Phys. Rev. D* **55**, 1280 (1997).
- [55] M. Gluck, E. Reya and A. Vogt, *Phys. Rev. D* **45**, 3986 (1992).
- [56] M. Gluck, E. Reya and M. Stratmann, *Phys. Rev. D* **51**, 3220 (1995).
- [57] L. Gladilin, hep-ex/9912064 (1999).
- [58] Particle Data Group, K. Hagiwara et al., *Phys. Rev. D* **66**, 010001 (2002).

W Range (GeV)	$d\sigma/dW \pm (\text{stat.}) \pm (\text{syst.})$ (nb/GeV)
130 - 160	$0.0226 \pm 0.0054^{+0.0067}_{-0.0025}$
160 - 188	$0.0214 \pm 0.0036^{+0.0027}_{-0.0004}$
188 - 226	$0.0111 \pm 0.0026^{+0.0008}_{-0.0007}$
226 - 280	$0.0080 \pm 0.0017^{+0.0007}_{-0.0017}$
$p_T(D^{*\pm})$ Range (GeV)	$d\sigma/dp_T(D^{*\pm}) \pm (\text{stat.}) \pm (\text{syst.})$ (nb/GeV)
1.9 - 2.3	$1.991 \pm 0.531^{+0.317}_{-0.421}$
2.3 - 2.73	$1.089 \pm 0.261^{+0.144}_{-0.168}$
2.73 - 3.8	$0.364 \pm 0.090^{+0.055}_{-0.018}$
3.8 - 15	$0.038 \pm 0.004^{+0.003}_{-0.004}$
$\eta(D^{*\pm})$ Range	$d\sigma/d\eta(D^{*\pm}) \pm (\text{stat.}) \pm (\text{syst.})$ (nb)
(-1.5) - (-0.72)	$0.914 \pm 0.126^{+0.087}_{-0.067}$
(-0.72) - (-0.15)	$0.858 \pm 0.147^{+0.164}_{-0.055}$
(-0.15) - (+0.42)	$0.665 \pm 0.161^{+0.222}_{-0.064}$
(+0.42) - (+1.5)	$0.436 \pm 0.132^{+0.061}_{-0.186}$
x_L Range	$d\sigma/dx_L \pm (\text{stat.}) \pm (\text{syst.})$ (nb)
0.2 - 0.46	$2.18 \pm 0.48^{+0.15}_{-0.20}$
0.46 - 0.64	$3.70 \pm 0.64^{+0.25}_{-0.34}$
0.64 - 0.82	$4.29 \pm 0.65^{+0.32}_{-0.42}$
0.82 - 1.0	$0.456 \pm 0.381^{+0.073}_{-0.086}$

Table 1: Values of the differential cross sections for neutron-tagged $D^{*\pm}$ photo-production ($Q^2 < 1 \text{ GeV}^2$ and $\theta_n < 0.8 \text{ mrad}$) with respect to W , $p_T(D^{*\pm})$, $\eta(D^{*\pm})$ and x_L .

W Range (GeV)	$r^{D^*} \pm (\text{stat.}) \pm (\text{syst.})$
130 - 160	$0.089 \pm 0.022^{+0.004}_{-0.055}$
160 - 188	$0.101 \pm 0.017^{+0.006}_{-0.025}$
188 - 226	$0.075 \pm 0.018^{+0.012}_{-0.004}$
226 - 280	$0.090 \pm 0.019^{+0.006}_{-0.022}$
$p_T(D^{*\pm})$ Range (GeV)	$r^{D^*} \pm (\text{stat.}) \pm (\text{syst.})$
1.9 - 2.3	$0.137 \pm 0.038^{+0.030}_{-0.007}$
2.3 - 2.73	$0.105 \pm 0.026^{+0.026}_{-0.005}$
2.73 - 3.8	$0.058 \pm 0.014^{+0.011}_{-0.003}$
3.8 - 15	$0.087 \pm 0.010^{+0.004}_{-0.009}$
$\eta(D^{*\pm})$ Range	$r^{D^*} \pm (\text{stat.}) \pm (\text{syst.})$
(-1.5) - (-0.72)	$0.093 \pm 0.013^{+0.005}_{-0.025}$
(-0.72) - (-0.15)	$0.097 \pm 0.016^{+0.007}_{-0.024}$
(-0.15) - (+0.42)	$0.085 \pm 0.021^{+0.007}_{-0.028}$
(+0.42) - (+1.5)	$0.080 \pm 0.024^{+0.004}_{-0.022}$

Table 2: Values of the ratios of the differential cross sections for neutron-tagged to inclusive $D^{*\pm}$ photoproduction ($Q^2 < 1 \text{ GeV}^2$, $x_L > 0.2$ and $\theta_n < 0.8 \text{ mrad}$) with respect to W , $p_T(D^{*\pm})$ and $\eta(D^{*\pm})$.

ZEUS

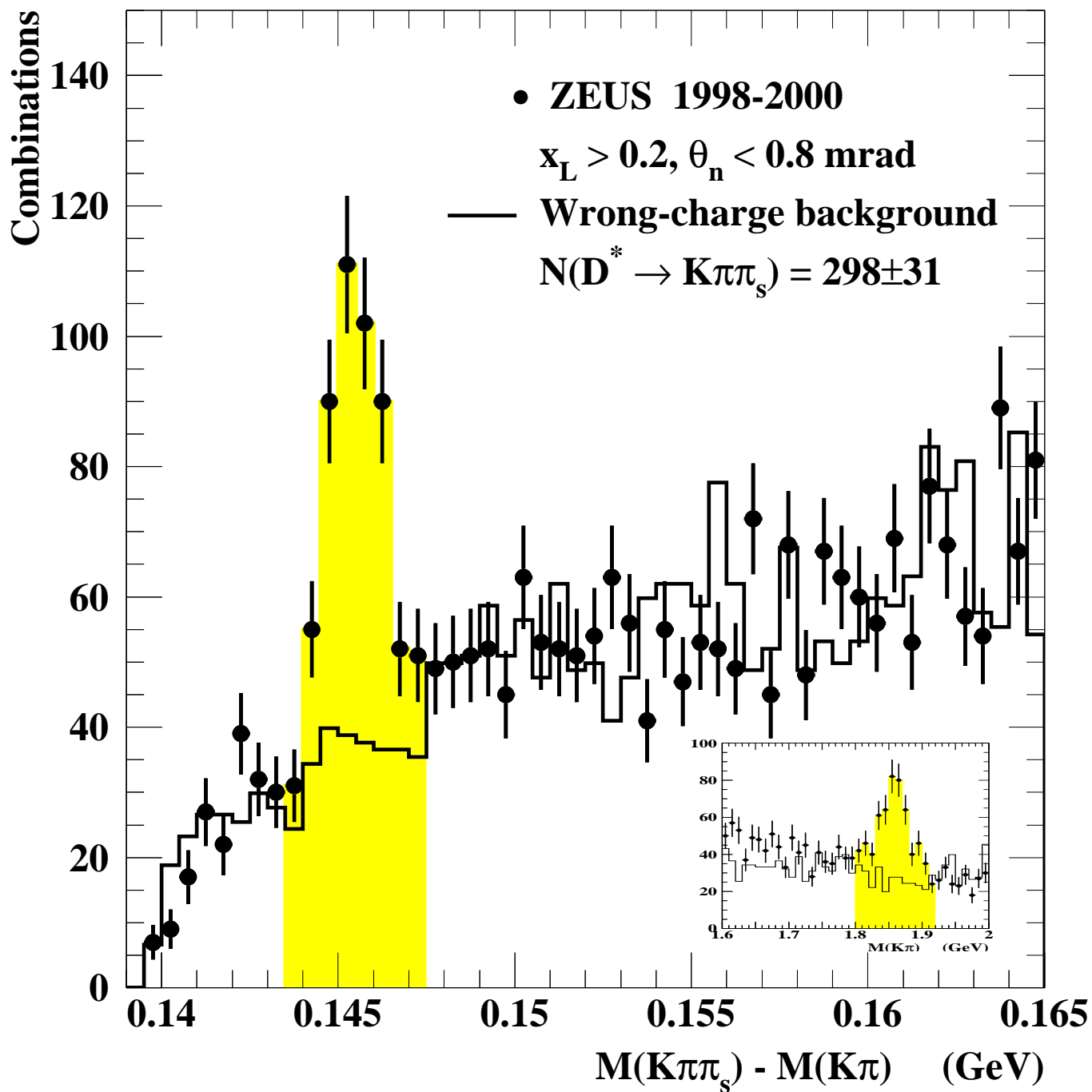


Figure 1: The data points show the neutron-tagged ΔM distribution for right-charge track combinations. The solid line shows the wrong-charge combinations normalized to the right-charge combinations in the region $0.15 < \Delta M < 0.165$ GeV outside the $D^{*\pm}$ mass window $0.1435 < \Delta M < 0.1475$ GeV which is shown shaded. The signal observed in the $M(K\pi)$ distribution for events within the mass window $0.1435 < \Delta M < 0.1475$ GeV is shown as an inset. The solid line also shows the wrong-charge combinations normalized to the right-charge combinations as before.

ZEUS

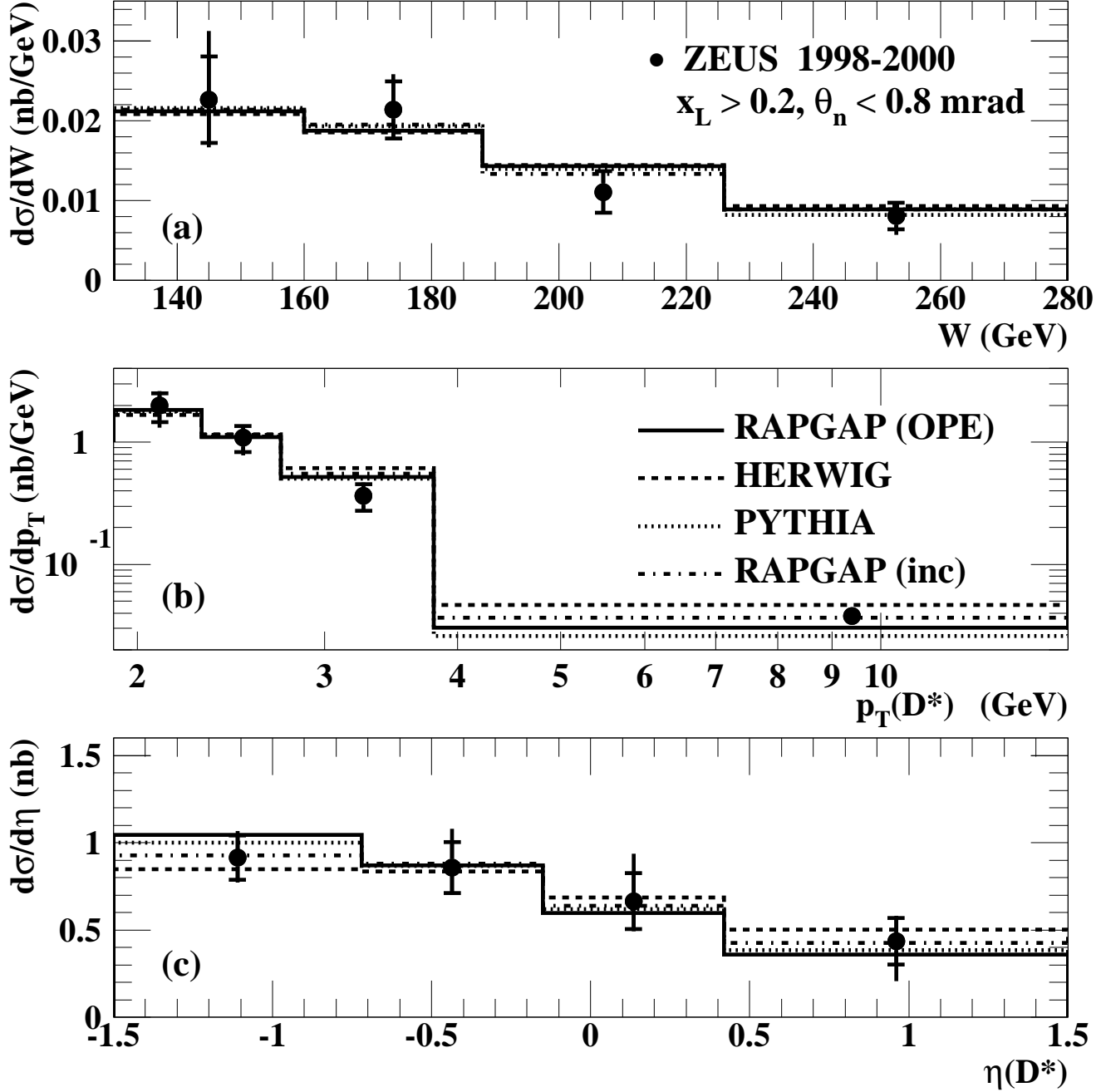


Figure 2: The points show the differential cross sections for neutron-tagged $D^{*\pm}$ production as a function of W , $p_T(D^*)$ and $\eta(D^*)$ for $x_L > 0.2$ and $\theta_n < 0.8$ mrad. The error bars displayed on the plots denote the statistical uncertainty (inner) and the quadratic sum of the statistical and the systematic uncertainties (outer). The uncertainties due to the luminosity measurement and the branching ratios are not shown. The predictions of Monte Carlo models normalized to the data are also shown.

ZEUS

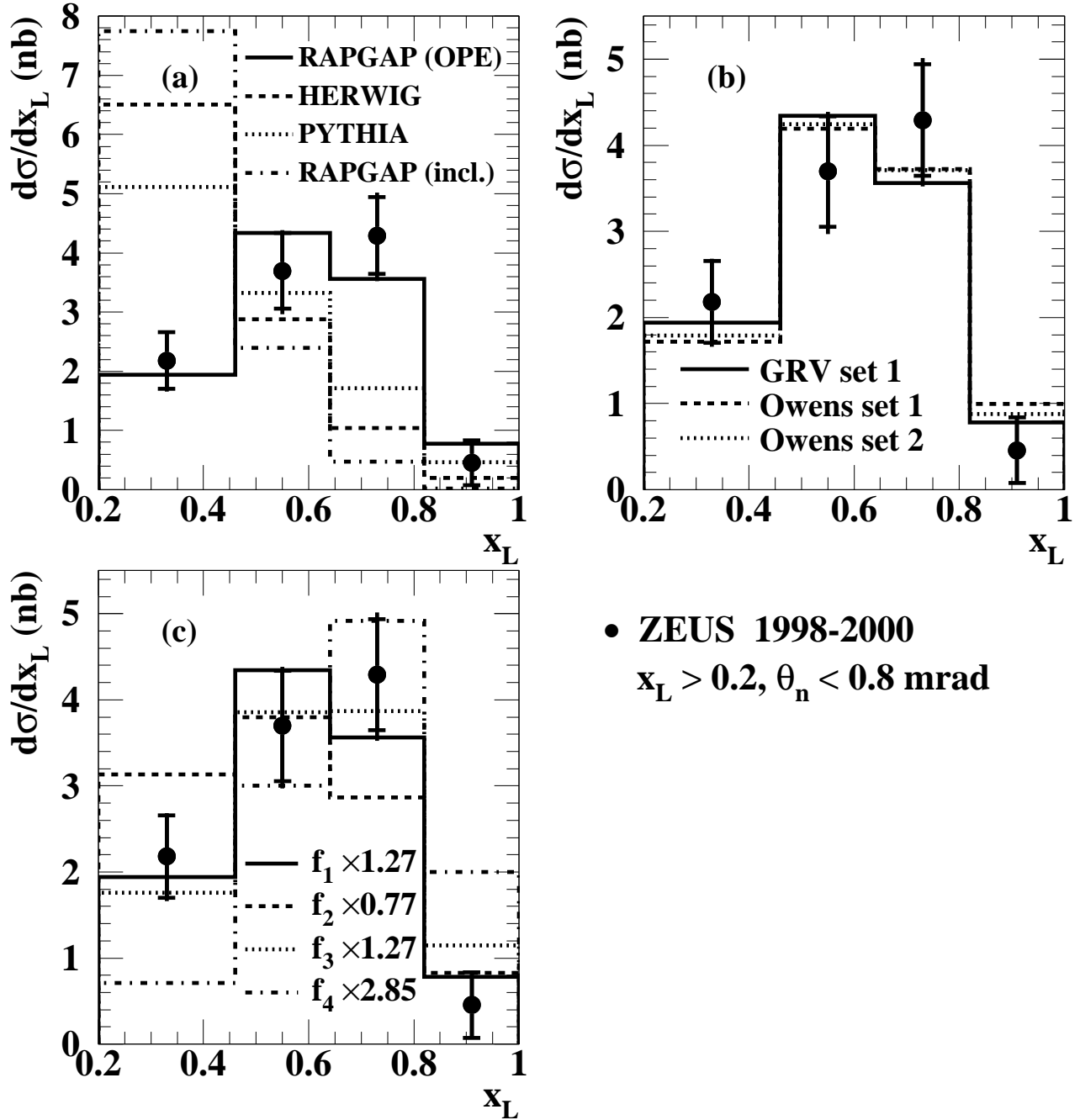


Figure 3: The points show the differential cross sections for neutron-tagged $D^{*\pm}$ production as a function of x_L . The histograms show the predictions of Monte Carlo models (a) RAPGAP with OPE (solid histogram), HERWIG (dashed), PYTHIA (dotted), and inclusive RAPGAP (dashed-dotted); (b) RAPGAP with OPE and pion PDF parametrizations from GRV set 1 (solid), Owens sets 1 (dashed) and 2 (dotted); (c) RAPGAP with OPE and flux factors f_1 - f_4 from Eqs. (3)-(4). The error bars displayed on the plots denote the statistical uncertainty (inner) and the quadratic sum of the statistical and the systematic uncertainties (outer). The uncertainties due to the luminosity measurement and the branching ratios are not shown. All distributions are normalized to the data. The numbers in (c) are the normalization factors.

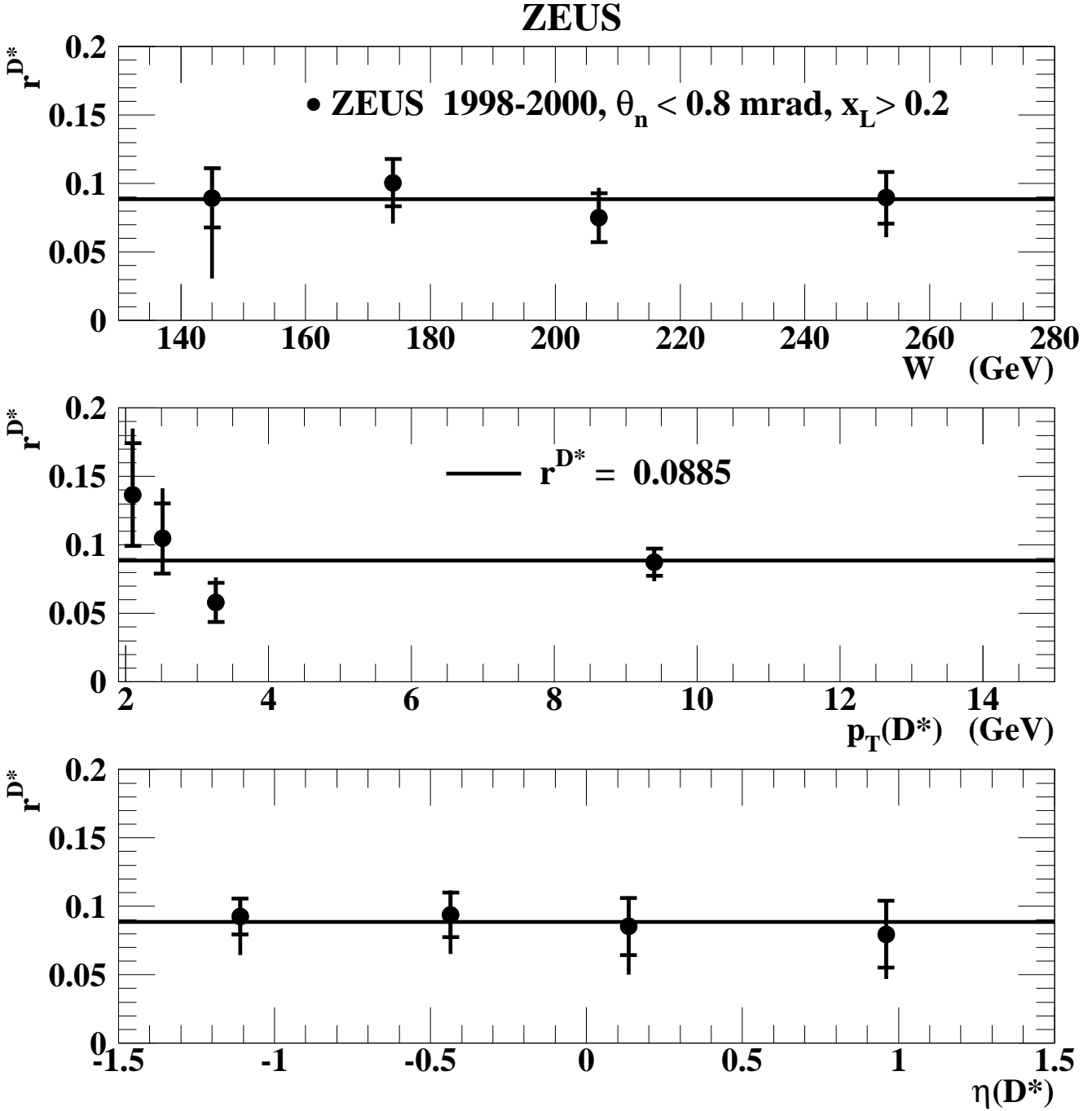


Figure 4: The ratio of neutron-tagged $D^{*\pm}$ production to inclusive $D^{*\pm}$ production as a function of W , $p_T(D^*)$ and $\eta(D^*)$ for $x_L > 0.2$ and $\theta_n < 0.8$ mrad. The error bars displayed on the plots denote the statistical uncertainty (inner) and the quadratic sum of the statistical and the systematic uncertainties (outer). The line superposed on the figures shows the overall ratio of neutron-tagged $D^{*\pm}$ to inclusive $D^{*\pm}$ events.